Drilling rate of five metals with picosecond laser pulses at 355, 532, and 1064 nm

Alex Spiro, Mary Lowe & Guerman Pasmanik

Applied Physics A
Materials Science & Processing

ISSN 0947-8396

Appl. Phys. A
DOI 10.1007/s00339-012-6910-x

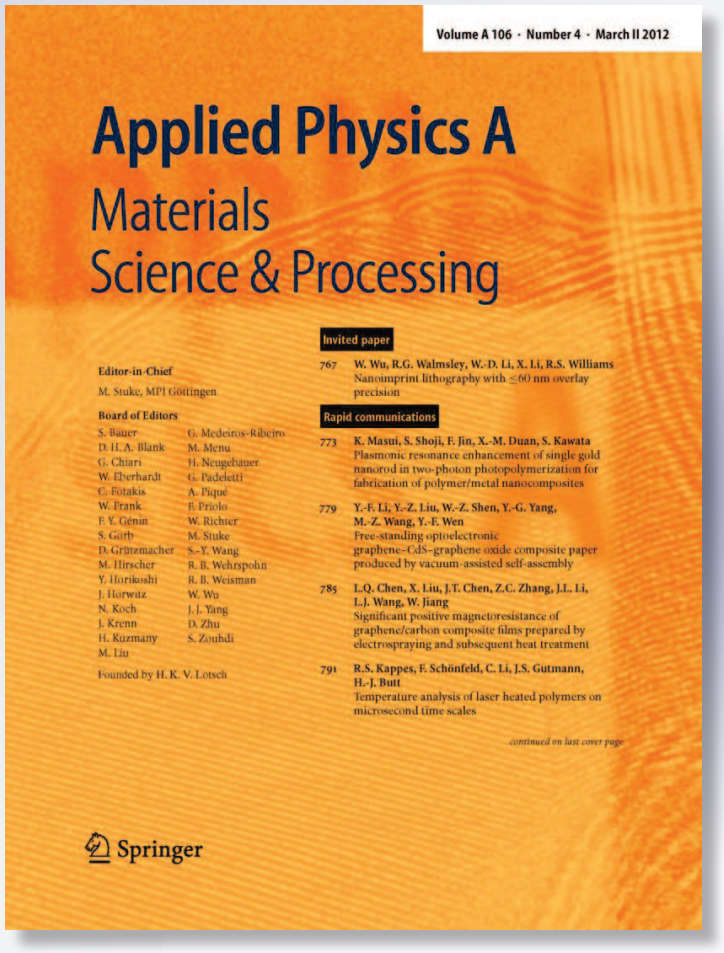

Springer

Appl Phys A
DOI 10.1007/s00339-012-6910-x

Applied Physics A
Materials Science & Processing

Drilling rate of five metals with picosecond laser pulses at 355, 532, and 1064 nm

Alex Spiro · Mary Lowe · Guerman Pasmanik

Received: 21 March 2012 / Accepted: 22 March 2012

Abstract Experimental results on picosecond laser processing of aluminum, nickel, stainless steel, molybdenum, and tungsten are described. Hole drilling is employed for comparative analysis of processing rates in an air environment. Drilling rates are measured over a wide range of laser fluences (0.05–20 J/cm^2). Experiments with picosecond pulses at 355 nm are carried out for all five metals and in addition at 532 nm, and 1064 nm for nickel. A comparison of drilling rate with 6-ps and 6-ns pulses at 355 nm is performed. The dependence of drilling rate on laser fluence measured with picosecond pulses demonstrates two logarithmic regimes for all five metals. To determine the transition from one regime to another, a critical fluence is measured and correlated with the thermal properties of the metals. The logarithmic regime at high-fluence range with UV picosecond pulses is reported for the first time. The energy efficiency of material removal for the different regimes is evaluated. The results demonstrate that UV picosecond pulses can provide comparable quality and higher processing rate compared with literature data on ablation with near-IR femtosecond lasers. A significant contribution of two-photon absorption to the ablation process is suggested to explain high processing rate with powerful UV picosecond pulses.

A. Spiro · G. Pasmanik (✉)
Passat, Inc., 1124 Kingsbury Rd., Owings Mills, MD 21117, USA
e-mail: guerman@passatltd.com
Fax: +1-888635-0657

M. Lowe
Loyola University Maryland, 4501 N. Charles St., Baltimore, MD 21210, USA

1 Introduction

The use of laser pulses for micromachining of metals has a number of important advantages over other fabrication techniques. In particular, drilling with sub-picosecond UV pulses enables structures to be made down to the submicron region with virtually no defects related to the heat-affected zone [1]. Important criteria to assess the utility and state of maturity of laser technology are the ablation threshold, speed, quality, and energy efficiency of processing. The main characteristics of ablation depend on the laser pulsewidth τ_p, the wavelength λ, the fluence F, and the material properties. The significance of pulsewidth on the ablation behavior of metals was clearly demonstrated in [2] where the ablation threshold in a Ni film with 0.5-ps UV pulses was 100 times lower than with 14-ns pulses of the same wavelength. The results of [2] and subsequent studies [1, 3–10] led to the generally accepted view that the lowest energy threshold and the best ablation quality are attainable with short (picosecond/femtosecond) pulses; the removal of material starts soon after laser irradiation with a minimal amount of melting. In contrast, with longer pulses, the heating, melting, and vaporization occur during the energy deposition that results in energy losses associated with heat conduction as well as with plasma development above the target [2, 5, 10, 11]. The presence of molten and boiling metal during the interaction reduces the quality of processing.

The obvious benefits of pulse shortening to reduce the threshold and improve ablation quality led to numerous investigations using femtosecond lasers operating mostly in the near-IR range. Two different regimes of metal ablation for low- and high-fluence ranges were observed for femtosecond pulses in [12] and then studied in more detail [6, 7, 13]. In terms of quality and mechanism of material removal, these two regimes can be characterized as

Published online: 11 April 2012

"gentle" and "strong" ablation phases [13], or as "non-thermal" and "thermal" ablation [6]. Above some critical pulsewidth τ_{cr}, the threshold fluence becomes dependent on τ_p [4]. The value τ_{cr} decreases with increasing F and at a given value of F, "thermal" ablation becomes dominant when $\tau_p > \tau_{cr}$ [6].

UV short pulses combine the advantages of high optical resolution with the ability to minimize the heat-affected zone [1]. In addition, the absorption coefficient of metals is generally higher in the UV range compared to that in the IR region, which should provide a lower ablation threshold for UV pulses. However, systematic studies of ablation of metals with UV pulses shorter than 1 ps are very small in number and are mainly represented by experiments with sub-picosecond excimer lasers [1–3]. The reason is that the conversion efficiency of radiation from existing solid-state near-IR femtosecond lasers into the UV region is limited by the self-focusing of the beam in nonlinear crystals, and by the large spectral width of ultrashort pulses. On the other hand, IR pulses of several picoseconds in length can be converted to UV with efficiency up to 50 % [14]. Comparative experiments between 10-ps UV and 10-ps IR laser pulses showed that for some metals, removal efficiency of the material at 355 nm is higher than at 1064 nm [15]. We believe that more detailed studies of the interaction of picosecond UV pulses with metals is of scientific interest and could be a good platform for the development of advanced technologies.

The present study is focused on comparing the material removal rate by drilling of five metals using UV pico- and nanosecond pulses at 355 nm over a wide range of fluences. In addition, experiments are presented on drilling one type of metal with a picosecond laser at 355, 532 and 1064 nm. Quantitative characterization of laser ablation of metals is dependent on the method of measurement and on the environmental conditions (air or vacuum) [2, 3, 13, 16]. In this study comparative experiments are conducted under the same environmental condition (air) using the same method, namely through-hole drilling. The results are compared with literature data on the ablation with femtosecond lasers.

2 Experimental setup and procedure

The experiments were performed with two types of commercial diode-pumped laser (Passat, Inc). The picosecond laser Compiler 355 is based on Raman shifting of nanosecond pulses at 1064 nm to the Stokes range with simultaneous time-compression followed by the anti-Stokes frequency shift back to the fundamental wavelength. The compressed picosecond pulse at 1064 nm is then amplified and frequency-converted in Compiler 355 to the second and third harmonics. The maximum repetition rate is 400 Hz. The laser emits pulses at 1064 nm (500 μJ, 8 ps), 532 nm (250 μJ, 7 ps) and 355 nm (150 μJ, 6 ps). The nanosecond model Naples-Compact is based on a Q-switched Nd:YAG laser with intra-cavity conversion to the third harmonic. The Naples-Compact delivers 6-ns pulses at a maximum repetition rate of 400 Hz with an average pulse energy of 200 μJ at 355 nm. For consistency in this study, both lasers were set at the same repetition rate: 200 Hz.

For all experiments with pico- and nanosecond lasers, the beams had a near Gaussian profile and a divergence close to the diffraction limit. The beams were focused by a fused silica lens with a focal length of 50 mm. Depending on the laser type and the wavelength, the beam diameter on the lens plane was within the range of 1.7–2 mm. The pulse energy was varied with a set of neutral filters and with an attenuator consisting of a rotary half-wave plate and a thin film dielectric polarizer. The laser spot size on the target was defined in each series of experiments with a set of thin pinholes typically passing about 50–70 % of the incident beam. When the laser spot size was measured in the plane of the sample, the pulse energy was minimized to prevent damage to the pinhole. Fluences were deduced by a Gaussian approximation of the spatial beam profile. The samples were positioned at two different distances behind the focal plane in order to provide two overlapping ranges of fluences. Depending on the laser type and the wavelength, the laser spot diameter (at $1/e^2$) was 100–130 μm in the first position and 25–60 μm in the second position (closer to the focus). The attenuator and filters varied the fluence within each range. Average drilling depth per pulse (drilling rate) was determined by counting the number of incident laser pulses during the drilling of each individual hole. Pulse counting was stopped at the first sign of an output laser beam behind the sample indicating the presence of a through-hole. The average depth per pulse was calculated from the total number of pulses and the sample thickness. Four to six holes in each sample were drilled at a given fluence level and the results were averaged.

Five metals were selected with different thermal characteristics: aluminum (Al, purity: 99.9 %), nickel (Ni, purity: 99.9 %), stainless steel (SS302, Fe/Cr18/Ni8), molybdenum (Mo, purity: 99.95 %) and tungsten (W, purity: 99.8 %). All samples had the same thickness of 100 μm.

3 Results

3.1 Drilling rate of five metals with pico- and nanosecond pulses at 355 nm

We tested the drilling rate on five metals using pico- and nanosecond UV pulses with variable incident peak fluences F_p from 0.05 to 20 J/cm^2. Due to possible variations of the

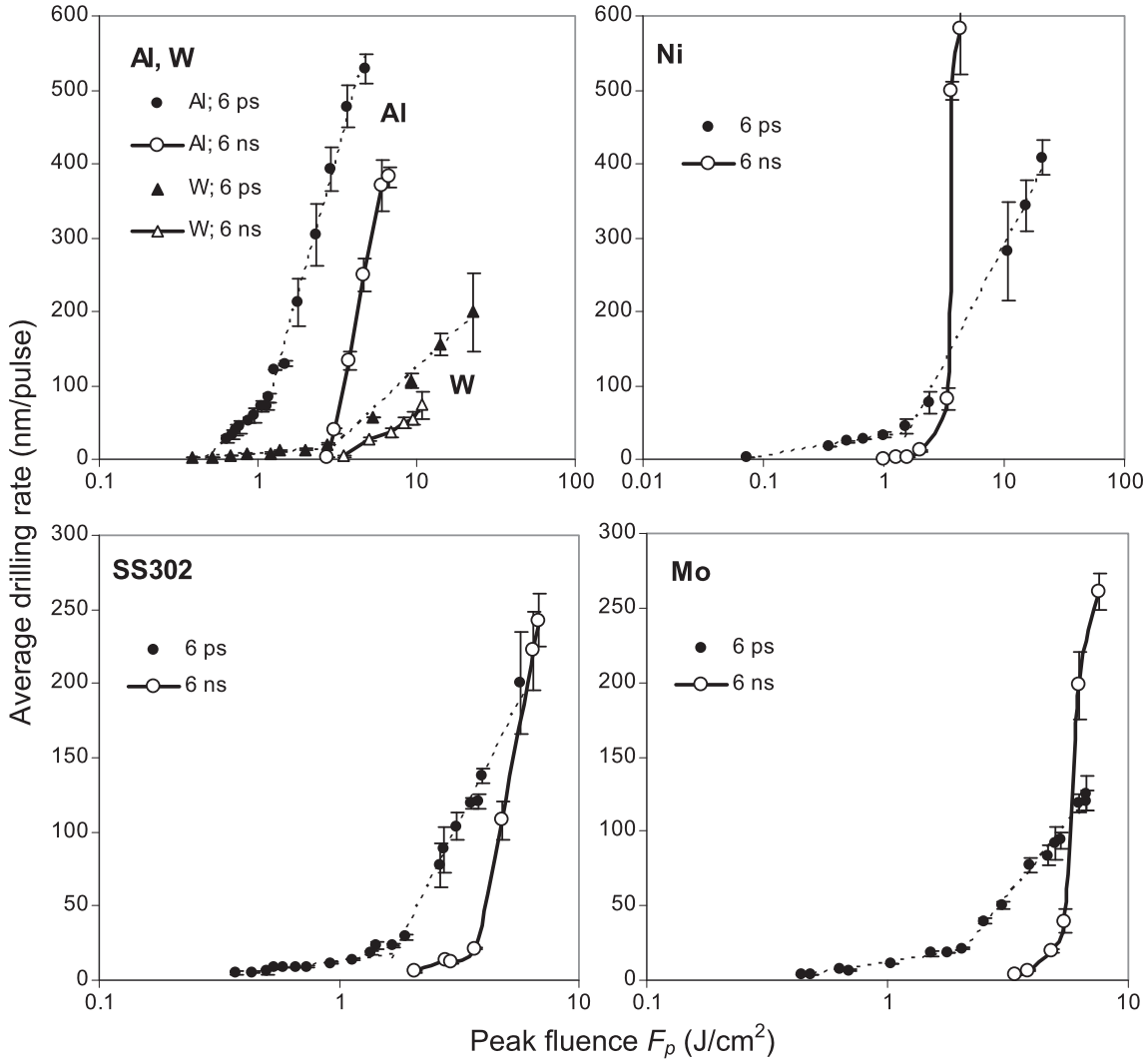

Fig. 1 Drilling rate vs. peak fluence for five metals using lasers at 355 nm: 6-ps pulses (●, ▲) and 6-ns pulses (○, Δ). The *dashed lines* illustrate the best fit using Eq. (1) for two logarithmic regimes

ablation depth for each individual pulse with the deepening of the hole, the results are presented in terms of average drilling rate. For low fluences, below 2 J/cm^2, the depth effect was assumed to be negligible because the laser beam diameter on the target was larger than or comparable to the depth of the through-hole (aspect ratio AR $\leq$ 1). With smaller spots (AR = 1.7−4), the fluence ranged from 1 to 20 J/cm^2. The depth effect was checked by using large (AR $\approx$ 1) and small (AR = 1.7–3) spots with the same range: $F_p = 1-2$ J/cm^2. Since no significant difference in the average drilling rate was observed with different spot sizes used in these experiments, we plotted all results on the same graph with no corrections for the aspect ratio.

Figure 1 compares the drilling rate for a range of fluences for five metals. Efficient drilling with nanosecond pulses occurs at much higher fluences compared to that of picosecond pulses. In contrast to ablation with picosecond pulses, the drilling rate with nanosecond pulses grows sharply with increasing fluence soon after reaching the threshold. According to [17], this can be attributed to the sharp transition from evaporation near the threshold to melt ejection when the absorbed power density is close to approximately 1 GW/cm^2 (6 J/cm^2 for 6 ns). The region of sharp increase in the curves for 6 ns in Fig. 1 moves towards higher fluences for metals with larger heat of fusion: Al (10.7 kJ/mol), Ni (17.5 kJ/mol), Mo (27.6 kJ/mol), and W (35.3 kJ/mol). The lattice is heated during the nanosecond pulse, so that instead of solid-gas ablation, vaporization occurs from the surface of the molten material even at lower intensities, and melt ejection is possible [17, 18]. Due to the sharp increase with high-energy nanosecond pulses, the drilling rate can be comparable or superior relative to that of picosecond pulses, as observed for Ni, SS302, and Mo.

In the curves shown in Fig. 1 for picosecond pulses, for each metal there are two regions with different slopes that can be attributed to two ablation regimes found in previous experiments using near-IR femtosecond lasers [7, 12, 13]. Theoretically, for each region the depth h removed with a single pulse can be determined from a well-known logarithmic law that reflects the exponential decay of deposited energy over the sample depth [3]. In a simplified form the dependence of h on the peak fluence F_p can be written as

$$h = l \ln(F_p/F_0) \quad (1)$$

where l and F_0 are the scaling parameters related to the energy penetration depth and to the threshold fluence, respectively. Using a logarithmic scale of fluences, this function is a straight line with slope l, where $h = 0$ when $F_p = F_0$. For each tested metal, two straight lines in Fig. 1 (for 6 ps) can be fit with different slopes and x-intercepts. The fitting parameters in Eq. (1) are designated as l_1 and $F_0^{(1)}$ for the low-fluence range (first regime) and as l_2 and $F_0^{(2)}$ for the high-fluence range (second regime). The fits using Eq. (1) are shown with dashed lines in Fig. 1 for all samples and are illustrated in more detail in Fig. 2 for tungsten. Table 1 summarizes the fitting parameters along with related literature data. The critical value of fluence F_{cr} characterizing the transition between the two regimes was calculated from the intersection of the corresponding fitting curves (Fig. 2). For simplicity the reflection from the surface [2, 3], the dependence of the ablation rate and the threshold on the number of pulses, the surface morphology, and the profile of ablated crater [13, 16, 19] are not considered.

For three metals Ni, Mo, and W the energy penetration depth l_1 in the first regime ($F_p < F_{cr}$) is close to the optical penetration depth defined from the absorption coefficient (Table 1). The value $F_0^{(1)}$ for Ni and W are in agreement with the fluence thresholds F_0 measured in vacuum with 0.5-ps pulses at 248 nm [3]. However, according to [7], the threshold for certain metals increases by about 2–3 times as the width of 800-nm pulses is increased from 0.1 to 4.5 ps, whereas in this work we did not see a significant difference between results observed with 6 ps UV pulses and results reported in [3]. For Mo, $F_0^{(1)}$ is about two times higher than the threshold for 0.5 ps UV pulses [3].

A surprisingly large penetration depth $l_1 \approx 84$ nm was obtained for Al in the low-fluence range. This depth is about

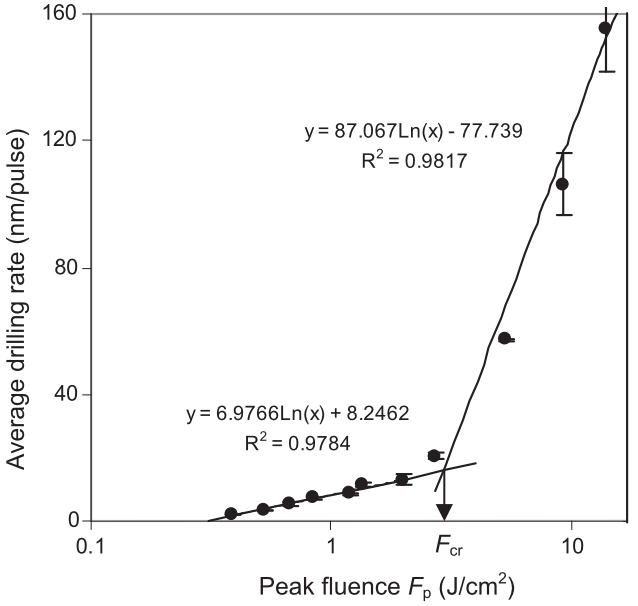

Fig. 2 Details of drilling rate of tungsten as a function of peak fluence. The *lines* represent best fits using Eq. (1) where $l_1 = 6.98$ nm and $F_0^{(1)} = 0.31$ J/cm^2 for the low-fluence range and $l_2 = 87$ nm and $F_0^{(2)} = 2.44$ J/cm^2 for the high-fluence range. The critical value $F_{cr} = 2.9$ J/cm^2 shows the fluence at the intersection point of the *fitting lines*

Table 1 Penetration depths l_1, l_2, threshold fluences $F_0^{(1)}$, $F_0^{(2)}$, and critical fluence F_{cr} obtained by fitting Eq. (1) to experiments with UV picosecond pulses. Literature data on ablation with femtosecond pulses for five metals are shown: (a) [7], (b) [3], and (c) [13]

Metal	1st regime		2nd regime			Literature data					
	l_1 (nm)	$F_0^{(1)}$ (J/cm^2)	l_2 (nm)	$F_0^{(2)}$ (J/cm^2)	F_{cr} (J/cm^2)	$1/\alpha$[a] (nm)	F_0[b] J/cm^2	τ_p (ps)	λ (nm)	Lit	Melting point (K)
Al	84.2	0.46	335	0.93	1.2	7.5	0.12	0.1	800	(a)	933
Ni	11.7	0.066	138	1.23	1.6	8	0.08	0.5	248	(b)	1728
SS	8.53	0.23	153	1.51	1.7		0.13	0.15	775	(c)	
Fe						18.3				(a)	1811
Mo	11.1	0.34	85.2	1.63	2.1	7.2	0.155	0.5	248	(b)	2896
W	6.98	0.31	87.1	2.44	2.9	7	0.4	0.5	248	(b)	3695

[a]The values represent the optical penetration depth calculated from absorption coefficient α

[b]The values represent the threshold fluence deducted from fitting of a logarithmic function to the experimental ablation rate measured at low fluences < 1.5 J/cm^2

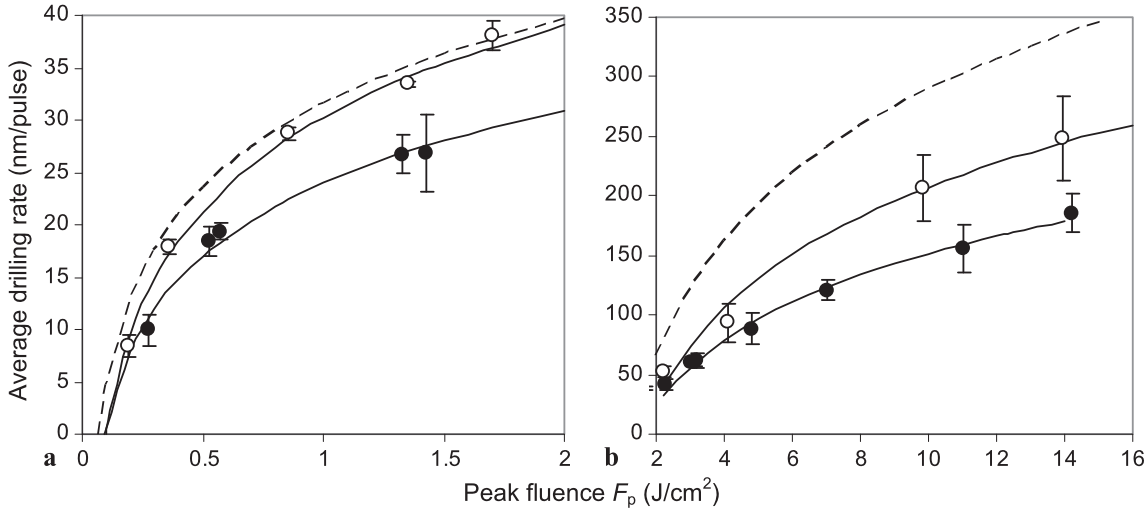

Fig. 3 Drilling rate of nickel vs. fluence for picosecond pulses at different wavelengths in (**a**) the first and (**b**) the second regimes. Laser wavelengths: 532 nm (○) and 1064 nm (●). The *solid lines* are the fit to Eq. (1). For comparison, the *dashed lines* show the fitting curves for picosecond pulses at 355 nm (Fig. 1 and Table 1)

11 times greater than that predicted by the reciprocal of the absorption coefficient. Unusual behavior of ablation curves for Al was also reported for short pulses at 800 nm in [7] and attributed to strong electron-phonon coupling. For the threshold fluence of Al, our result of $F_0^{(1)} = 0.46$ J/cm^2 is similar to the result for 10-ps pulses at the same wavelength, where $F_0 \approx 0.35$ J/cm^2 [15]. In stainless steel the value of l_1 is lower than the optical penetration depth in iron, while $F_0^{(1)}$ is higher than the ablation threshold at low fluences for near-IR femtosecond pulses [13]. Differences in optical properties among various types of steel make it difficult to compare our data with ablation characteristics reported in the literature.

In the second regime, the values of $F_0^{(2)}$ for stainless steel (1.51 J/cm^2) and Al (0.93 J/cm^2) are close to the threshold values reported for 100–150 fs near-IR pulses for SS (1.1–1.25 J/cm^2) [7, 13] and for Al (about 0.8 J/cm^2) [7]. As shown in [7], the threshold fluence values slightly increase (within 30 %) with increasing pulse duration from 0.1 to 4.5 ps, while the penetration depth decreases from about 300 nm to 120 nm for SS and from about 160 nm to 70 nm for Al. In this work, the penetration depth measured with 6-ps UV pulses is $l_2 \approx 150$ nm for SS, which according to [7] corresponds to the result for 3–4-ps pulses at 800 nm. The value of $l_2 \approx 330$ nm for Al (Table 1) is larger than the results for 100-fs and 4.5-ps near-IR pulses [7].

For both femto- and picosecond pulses there is no clear correlation between the ablation threshold at low fluences (parameters F_0 and $F_0^{(1)}$ in Table 1) and melting temperature. There is a clear proportionality between the critical fluence F_{cr} and the melting temperature. Also, the energy penetration depth l_2 in the second regime ($F_p > F_{cr}$) is higher in pure metals with lower melting temperature.

Table 2 Parameters l_1, $F_0^{(1)}$, l_2, $F_0^{(2)}$, and F_{cr} obtained from fitting Eq. (1) to experiments on drilling nickel with picosecond pulses at three wavelengths

λ (nm)	1st regime		2nd regime		
	l_1 (nm)	F_0^1 (J/cm^2)	l_2 (nm)	F_0^2 (J/cm^2)	F_{cr} (J/cm^2)
355	11.7	0.066	138	1.23	1.60
532	13	0.096	110	1.53	2.21
1064	10	0.092	79	1.47	2.24

3.2 Drilling rate in nickel with picosecond pulses at 532 and 1064 nm

To compare processing speeds for different wavelengths, we conducted drilling experiments on nickel with a picosecond laser Compiler 355. The beam at operating wavelength was extracted from the laser before conversion to a higher harmonic. Figure 3 shows the drilling rate for varying peak fluences at 1064 and 532 nm. These rates are compared with the results described above for 6-ps 355-nm pulses.

The experimental dependences were approximated with a logarithmic function (Eq. (1)). As in the case of 355-nm pulses, there are two regimes with different parameters l and F_0 (Table 2). In the low- and high-fluence ranges, the drilling rate for UV is higher than that at longer wavelengths (Fig. 3). In the high-fluence range (Fig. 3b), deeper energy penetration for 355 nm pulses is probably associated with higher electronic temperature due to the high energy of absorbed UV photons. In the low-fluence range $F_p < 2$ J/cm^2 (Fig. 3a), the drilling rate is higher for 355 nm than for 1064 nm because the threshold fluence is lower. The pene-

tration depth l_1 for all three wavelengths is 10–13 nm, which is close to the optical penetration depth $\alpha^{-1} \approx 8$ nm [8]. In general, for picosecond pulses the processing rate for shorter wavelengths exceeds the processing rate for longer wavelengths. This difference becomes more pronounced at higher fluences, while for nanosecond pulses the reverse situation is possible [20, 21].

3.3 Energy efficiency of drilling

An important aspect in laser micromachining is the energy efficiency of processing, which shows the amount of material removed per unit of laser energy. The maximum possible efficiencies can be estimated from our data with three simplifying assumptions: (i) the laser beam has a flat-top intensity distribution with the same fluence F_p in each point, (ii) the ablated cavity has a flat-bottomed shape and a cross-section that reproduces the beam shape, and (iii) the ablation depth h is identical for each pulse of the same energy. These assumptions approach reality in the center of Gaussian beam, where the peak fluence F_p ablates the depth h. Then the maximum possible energy efficiency $\xi = h/F_p$ represents the volume of ablated material per unit of incident energy. These simplifications allow the optimal regime of processing to be chosen. When the ablation depth h per pulse obeys the logarithmic law (Eq. (1)), the dependence of ξ on fluence takes the form

$$\xi = (l/F_p)\ln(F_p/F_0). \quad (2)$$

Figure 4 shows ξ (in units of mm^3/J) as a function of fluence, where ξ is calculated based on the data shown in Figs. 1 and 3. The function $\xi = f(F_p)$ in Eq. (2) has a maximum $\xi_{max} = l/(F_{max})$ at $F_{max} = eF_0 = 2.72F_0$. Since two logarithmic regimes are identified for drilling with picosecond pulses, ξ has two maxima as illustrated in Fig. 4 for Ni, Mo, and W. UV pulses are more efficient compared to IR pulses as demonstrated by Ni over both regimes. For comparison Fig. 4 also shows the values of ξ obtained from tungsten with 6-ns pulses at 355 nm. The solid lines represent $\xi = f(F_p)$ using the parameters l_1, $F_0^{(1)}$, l_2, and $F_0^{(2)}$ from Table 1. In the case of Ni (6 ps, 355 nm) the main maximum $\xi_{max} = l_1/(eF_0^{(1)}) = 0.0064$ mm^3/J is in the first regime because of the lower threshold value $F_0^{(1)}$, while the other metals have the main maximum in the second regime.

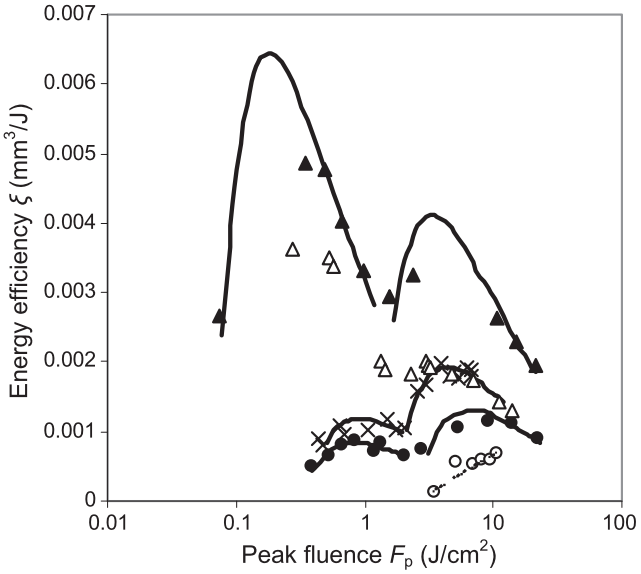

Fig. 4 Energy efficiency of material removal. The target, pulse duration, and wavelength are: Ni, 6 ps, 355 nm (▲); Ni, 6 ps, 1064 nm (△); Mo, 6 ps, 355 nm (×); W, 6 ps, 355 nm (●); and W, 6 ns, 355 nm (○). The *solid lines* are the functional dependences $\xi = f(F_p)$ calculated using Eq. (2) with the fitting parameters shown in Table 1. Al and SS302 also exhibit two maxima with picosecond pulses. The main maxima are $\xi_{max} = l_2/(eF_0^{(2)}) = 0.0132$ mm^3/J (Al) and 0.0035 mm^3/J (SS302) at $F_{max} = 2.53$ J/cm^2 and 4.1 J/cm^2, respectively

4 Discussion

There are varying views on the existence of a low-fluence regime with short pulses in the literature. The estimates [2] showed that the thermal diffusion length in Ni is smaller than the optical penetration depth α^{-1} (at 248 nm) when the pulsewidth is shorter than 1.5 ps; the ablation is governed by the absorption coefficient α. In accordance with this, the experiments [12] for laser ablation of copper at 780 nm led to the conclusion that the ablation regime, determined by the exponential decay of laser light, is only possible with pulses shorter than 1 ps. In contrast, a low-fluence regime was observed for Al, Cu, and steel when the energy penetration depth is close to α^{-1} for near-IR pulses up to 4.5 ps [7]. In this work, well-defined low-fluence regimes were observed for 6 ps UV pulses (Figs. 1 and 2), where the energy penetration depth l_1 is close to the values of α^{-1} for four out of five samples, namely Ni, SS302, Mo, and W (Table 1).

In a prior study [2], the results of laser ionization time-to-flight mass spectrometry indicated vaporization of atoms from a Ni surface that was irradiated with 0.5-ps UV pulses at fluences as low as 0.02 J/cm^2. In other experiments with picosecond IR pulses and SEM imaging [6], the ablation of Al in the low-fluence regime was attributed to the mechanical separation and ejection of material due to a huge temperature gradient in a small volume. In our work, in which the hole-drilling method was employed, we did not find a clear correlation between the threshold of the low-fluence regime $F_0^{(1)}$ and evaporation or melting properties of the tested materials. The evaporation observed in [2] at very low fluence is below our detection limit. We believe that within the range between $F_0^{(1)}$ and critical fluence F_{cr}, effects of drilling associated with melting or boiling are minimal in accordance with [6].

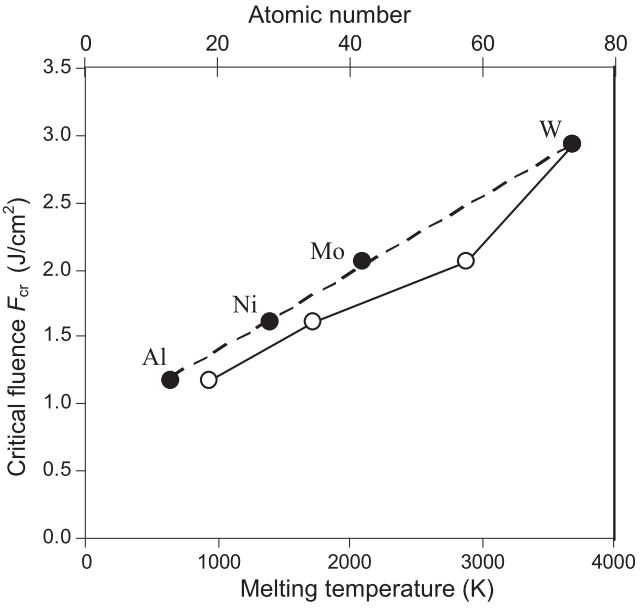

Fig. 5 Critical fluence for pure metals as a function of melting temperature (○) and of atomic number (●)

The values of F_{cr} for pure metals in Table 1 increase with the melting temperature, and interestingly is a linear function of the atomic number (Fig. 5). The latter may be a coincidence for the four selected metals. The dependence of the critical fluence on the melting temperature indicates the presence of a liquid phase in the ablation process for the high-fluence regime at $F_p > F_{cr}$.

The effect of electronic heat conduction considered in [7, 12, 13] for high-energy short near-IR pulses may be even greater with UV pulses, due to higher energy of photons with shorter wavelength. This assumption can be illustrated with the data of Fig. 3, which compares drilling rate for nickel measured with picosecond pulses at different laser wavelengths. In the range of high fluences $F_p > F_{cr}$, the energy penetration depth $l_2 \approx 140$ nm for 355-nm pulses is about two times larger than $l_2 \approx 78$ nm for 1064-nm pulses (Table 2). Also, the values of l_2 in aluminum and steel for 6-ps 355-nm pulses (Table 1) is greater than the penetration depth obtained for these metals in [7] with high-energy pulses at 800 nm of comparable duration (4.5-ps).

The above comparison for the high-fluence regime shows a greater processing rate using UV pulses compared to near-IR pulses. For example at a fluence of 5 J/cm^2 the drilling rate in Al measured in this work with 6-ps UV pulses (Fig. 1) is about 4.5 times higher than the ablation rate for 100-fs pulses at 800 nm [7]. This difference can be explained by higher two-photon absorption (TPA) in the UV range. A dominant contribution of nonlinear absorption to the ablation of dielectrics with short UV pulses is well studied [22, 23]. In the case of metal ablation with low-energy UV short pulses, multiphoton absorption is considered to be negligible compared to linear absorption [2, 3]. However, at high fluences of picosecond UV pulses, we suggest that the contribution of TPA can be significant and may exceed the contribution from linear absorption. Nonlinear optical susceptibility, which determines the coefficient of TPA (in cm/W), is proportional to the concentration of ions or molecules. The concentration of ions in metals typically exceeds the concentration of molecules in polymers, such as PMMA used in the TPA study [23]. According to our preliminary estimates, the density of UV energy (per cm^3) absorbed in the vicinity of the surface may exceed the value required for photo-destruction of the material via TPA.

In the case of nanosecond pulses, ablation is governed by the heat penetration depth $l_h \approx (2k\tau_p)^{-1/2}$ [2], where k is the thermal diffusivity and τ_p is the pulse length. A rough estimate based on the slope of the straight solid line for Al in Fig. 1 (355 nm, 6 ns) shows the penetration depth $l \approx 0.5$ μm, which is two times less but still of the same order of magnitude as the calculated value for $l_h \approx 1$ μm for 6 ns pulses ($k = 0.98$ cm^2/s for Al). Correct analysis requires much higher fluences than those used in this work, which focuses on a comparison with picosecond results. We believe that better ablation quality with nanosecond pulses can be achieved near the threshold fluence: $F_p < 3$ J/cm^2 for Ni, $F_p < 3.5$ J/cm^2 for SS302, $F_p < 5$ J/cm^2 for Mo, and $F_p < 9$ J/cm^2 for W. However, the processing rate in these cases is several times lower than that demonstrated with picosecond pulses.

5 Conclusion

With UV picosecond pulses, we demonstrated two different regimes of ablation for five metals. The drilling rate in both regimes can be approximated by a logarithmic dependence on the laser fluence F, but with different parameters for low and high ranges of F. For three metals, Ni, Mo, and W, the existence of the second logarithmic regime associated with high fluences was observed for the first time. The processing rate for UV picosecond pulses is faster than that for picosecond pulses at longer wavelength. Comparative analysis of our results with literature data suggests that the mechanism of ablation with UV picosecond pulses is similar to that achievable with near-IR femtosecond lasers.

In comparison with femtosecond pulses, this work suggests that comparable rate and quality of processing can be achieved with picosecond lasers. In additional we believe that in the case of high-energy short UV pulses, TPA can contribute to ablation efficiency. The high optical resolution and ablation quality make the picosecond UV laser an effective tool for producing fine microstructures.

For higher energy efficiency of material removal with picosecond lasers, UV pulses with moderate energies below 6–7 J/cm^2 in both regimes should be used. We have made

the first observation that for picosecond pulses the energy efficiency in the tested metals (except Ni) is approximately two times higher in the second regime than that in the first regime. At higher fluences $F_p > 10$ J/cm^2, processing efficiency with nanosecond lasers can be higher than with picosecond lasers. However, the presence of a significant amount of molten material during metal interaction with long pulses reduces the ablation quality.

Acknowledgements We wish to thank Joseph d'Entremont and Greg Solyar at Lenox Laser for hosting A.S. and use of the equipment.

References

1. J. Bekesi, J.-H. Klein-Wiele, P. Simon, Appl. Phys. A **76**, 355 (2003)
2. S. Preuss, E. Matthias, M. Stuke, Appl. Phys. A **59**, 79 (1994)
3. S. Preuss, A. Demchuk, M. Stuke, Appl. Phys. A **61**, 33 (1995)
4. J. Byskov-Nielsen, J.-M. Savolainen, M.S. Christensen, P. Balling, Appl. Phys. A **103**, 447 (2011)
5. Tunnermann, S. Nolte, J. Limpert, Laser Tech. J. **7**, 34 (2010)
6. J. Yang, Y. Zhao, N. Zhang, Y. Liang, M. Wang, Phys. Rev. B **76**, 165430-1 (2007)
7. R. Le Harzic, D. Breitling, M. Weikert, S. Sommer, C. Föhl, S. Valette, C. Donnet, E. Audouard, F. Dausinger, Appl. Surf. Sci. **249**, 322 (2005)
8. C.Y. Chien, M.C. Gupta, Appl. Phys. A **81**, 1257 (2005)
9. B.N. Chichkov, C. Momma, S. Nolte, F. von Alvensleben, A. Tunnermann, Appl. Phys. A **63**, 109 (1996)
10. Semerok, B. Sallé, J.-F. Wagner, G. Petite, Laser Part. Beams **20**, 67 (2002)
11. M.R.H. Knowles, G. Rutterford, D. Karnakis, A. Ferguson, Int. J. Adv. Manuf. Technol. **33**, 95 (2007)
12. S. Nolte, C. Momma, H. Jacobs, A. Tünnermann, B.N. Chichkov, B. Wellegehausen, H. Welling, J. Opt. Soc. Am. B **14**, 2716 (1997)
13. P.T. Mannion, J. Magee, E. Coyne, G.M. O'Connor, T.J. Glynn, Appl. Surf. Sci. **233**, 275 (2004)
14. T. Zhang, Y. Kato, H. Daido, IEEE J. Quantum Electron. **32**, 127 (1996)
15. R. Penttilä, H. Pantsar, P. Laakso, in *Proc. of the 11th NOLAMP Conf. in Laser Process. of Mater.* (Lappeenranta University of Technology, Lappeenranta, 2007), p. 502
16. A.E. Wynne, B.S. Stuart, Appl. Phys. A **76**, 373 (2003)
17. C. Körner, R. Mayerhofer, M. Hartmenn, H.W. Bergman, Appl. Phys. A **63**, 123 (1996)
18. N.M. Bulgakova, A.V. Bulgakov, Appl. Phys. A **73**, 199 (2001)
19. J. Byskov-Nielsen, J.-M. Savolainen, M.S. Christensen, P. Balling, Appl. Phys. A **101**, 97 (2010)
20. S. Amoruso, Appl. Phys. A **69**, 323 (1999)
21. Vladoiu, M. Stafe, C. Negutu, I.M. Popescu, J. Optoelectron. Adv. Mater. **10**, 3177 (2008)
22. S. Küper, M. Stuke, Appl. Phys. Lett. **54**, 4 (1989)
23. S. Preuss, M. Späth, Y. Zhang, M. Stuke, Appl. Phys. Lett. **62**, 3049 (1993)